SCIENCE CHINA
Technological Sciences

Modelling envelope and temporal fine structure components of frequency-following responses in rat inferior colliculus

WANG Qian and LI Liang

Citation: SCIENCE CHINA Technological Sciences **60**, 966 (2017); doi: 10.1007/s11431-016-9044-5

View online: http://engine.scichina.com/doi/10.1007/s11431-016-9044-5

View Table of Contents:http://engine.scichina.com/publisher/scp/journal/SCTS/60/7

Published by the Science China Press

SCIENCE CHINA

Cr

doi: 10.1007/s11431-016-9044-5

• Article •

Modelling envelope and temporal fne structure components of frequency-following responses in rat inferior colliculus

WANG Qian[1,2] & LI Liang[1,3,4*]

[1] *School of Psychological and Cognitive Sciences and Beijing Key Laboratory of Behavior and Mental Health, Peking University, Beijing 100871, China;*
[2] *Beijing Key Laboratory of Epilepsy, Epilepsy Center, Department of Functional Neurosurgery, Sanbo Brain Hospital, Capital Medical University, Beijing 100093, China;*
[3] *Speech and Hearing Research Center, Key Laboratory on Machine Perception (Ministry of Education), Peking University, Beijing 100871, China;*
[4] *Beijing Institute for Brain Disorders, Beijing 100081, China*

Received December 24, 2016; accepted March 27, 2017; published online June 20, 2017

In studies of auditory perception, a dichotomy between envelope and temporal fne structure (TFS) has been emphasized. It has been shown that frequency-following responsehavi [illegible] 1431-016-9044-5

of neuron populations to instantaneous waveforms of low-to-middle-frequency acoustic stimuli [12−20]. Previous studies had shown that FFRs can efficiently convey both TFS signals [12,14,21−25] and envelope signals (also called envelope-following response) [25−31]. As FFRs have been thought to be mainly originated from the auditory midbrain (i.e. inferior colliculus, IC) [12,13,18,32,33], our recent studies have also further suggested a functional dichotomy of the envelope component of FFR (FFR_{Env}) and the temporal fine structure component of FFR (FFR_{TFS}) in the rat IC [25].

Computational models for the generation of FFR are critical for understanding the properties of FFR, based on the neurophysiological parameters along the ascending pathway. Up to date, there are two existing FFR models. One has been established for human scalp FFRs [34] by convoluting click-evoked waveforms with the instantaneous discharge rates based on nonlinear cochlear processing [35]. Dau's FFR model (FFR) predicts well for the frequency dependent latency and intensity effect, but fails to simulate binaural response properties raised from brainstem nuclei.

The other one has been established for extracellular field potentials in owl's medial superior olivary nuclei (MSO) [36] by convolving Poisson processed spike trains with a model spike waveform. Although Kuokkanen et al.'s [36] FFR model solved the interaural processing pattern by linear summation of ipsilateral and contralateral input, some properties such as nonlinear cochlear processing or cellular properties are ignored. Thus, neither of these two models can separate FFR_{Env} and FFR_{TFS}.

Can different cellular properties of IC neurons be used to distinguish FFR_{Env} from FFR_{TFS}? The temporal processing properties of IC neurons can be described by modulation transfer functions (MTFs), which include several types [37]. A recent computational model has shown that activations of IC neurons with different types of MTFs can be effectively tuned to signal fluctuations [38]. More specifically, IC neurons with bandpass MTFs tune to slowly fluctuated amplitude modulations while neurons with band-reject or low-pass MTFs tune to quickly fluctuated vowel formants. These findings imply that the MTF types of IC neurons can be used to establish an IC FFR model which effectively separates FFR_{Env} and FFR_{TFS}.

On the purpose to develop an appropriate IC FFR model, we combined the advantages of these two existing FFR models [34,36], and simultaneously added a construction of MTF types IC neurons to simulate the separated envelope and TFS information processing [38]. To evaluate the validity of the current model, narrowband noise evoked intracranial FFRs were recorded in rat IC. Different model parameters were tested, correlations between simulated FFRs and experimental FFRs were calculated, and the parameters with highest prediction were chosen to build an ideal FFR model.

2 Methods

2.1 FFR recording

Intracranial IC FFRs were measured in 12 young-adult male Sprague-Dawley rats (age 10−12 weeks, weight 280−350 g). All rats were treated in accordance with both *the Guidelines of the Beijing Laboratory Animal Center* and *the Policies on the Use of Animal and Humans in Neuroscience Research* approved by the Society for Neuroscience (2006).

During the recording, rats were anesthetized with 10% chloral hydrate (400 mg/kg, intraperitoneal) and the state of anesthesia was maintained throughout the experiment by supplemental injection of the same anesthetic. Stainless steel recording electrodes (10−20 kΩ), which were insulated by a silicon tube (0.3 mm in diameter) except at the 0.25 mm diameter tip [13,15,25], were aimed at the central nucleus of the IC bilaterally. Based on the stereotaxic coordinates of ref. [39] and referenced to *Bregma*, the IC coordinates were: AP, –8.8 mm; ML, ±1.5 mm; DV, −4.5–−5.0 mm.

Gaussian wideband noises (10-kHz sampling rate and 16-bit amplitude quantization) were generated and filtered by a 512-point digital filter with a center frequency of 2000 Hz and a bandwidth of 0.466 octaves (ranged from 1680 to 2320 Hz) with MATLAB (MathWorks, Natick, MA, USA). The stimulus duration was 700 ms with 10-ms linear onset/offset ramps, and the (offset-onset) inter-stimulus interval was 100 ms. All sound waves were re-processed by a TDT System II (Tucker-Davis Technologies, FL, USA), and presented through two ED1 earphones. Two 12-cm TDT sound-delivery rubber tubes were connected to the ED1 earphones and inserted into each of the rat's ear canals for sound delivery. All narrow-band noises were calibrated using a Larson Davis Andiometer Calibration and Electroacoustic Testing System (AUDitTM and System 824, Larson Davis, USA). The level of all signals was 72 dB SPL for each earphone.

Evoked neural potentials were recorded in a sound-attenuating chamber, amplified 1000 times by TDT DB4 amplifer, filtered through a 100–10000 Hz band-pass filter (with a 50-Hz notch), and averaged 100 times per stimulus condition. Online recordings were processed with TDT Biosig software, digitized at 16 kHz, and stored on disk for off-line analyses. Stimuli were delivered to rats monaurally (either ipsilaterally or contralaterally).

When all recordings were completed, rats were euthanized with an overdose of chloral hydrate. Lesion marks were made via the recording electrodes by an anodal DC current (500 μA for 10 s). The brains were stored in 10% formalin with 30% sucrose, and then sectioned at 55 μm in the frontal plane in a cryostat (−20°C).

Theoretically, a steady-state Gaussian narrowband noise with a center frequency of c Hz and a bandwidth of b Hz has a TFS energy around c Hz and an envelope energy within

the frequency range between 0 and b Hz [40]. Thus, for a narrowband noise with bandwidth 640 Hz, the envelope spectrum were ranged from 0 to 640 Hz, while the TFS spectrum were ranged from 1680 to 2320 Hz. In that case, low-pass and high-pass FIR filters with 1000 Hz cut-off frequency were designed by the MATLAB fir2 function (512th-order) to extract the FFR_{TFS} and FFR_{Env} components from the original potential, respectively.

2.2 FFR modeling

As shown in Figure 1, the current FFR model in the present study mainly contented 5 steps. (1) The incoming stimulus was firstly processed through the newest computational auditory nerve (AN) [41]. This phenomenological AN model included several key nonlinearities, rate saturation, adaptation, and synchrony capture. (2) The second stage used two different rMTF functions (band-pass, BP; band-reject, BR) to separate the envelope and TFS responses [38]. (3) Then, the outputs from the second stage, instantaneous discharge rate along frequency channels, were produced by the fast-Poisson process [42] to generate spike trains. (4) The spike train in each frequency channel was then convolved with a model spike waveform k, which was approximated with a Gabor function [36].

$$k(t) \propto \exp\left(-\frac{t^2}{2\rho^2}\cos\left(2\pi f_g t + \phi\right)\right), \quad (1)$$

where width ρ = 0.09 ms, primary phase ϕ= 0.8 rad, oscillation frequency f_g =3.9 kHz. The absolute peak amplitude was set to 100 μV. (5) The fourth stage mentioned above was generated independently by 100 times. The simulated FFR potentials were generated by summing the output of each CF channels, with 100 repetitions.

Narrowband noise with sound level of 72 dB SPL, center frequency of 2000 Hz, and bandwidth of 640 Hz, which was used to evoke the experimental FFR in the present study was entered into the model. The fixed model parameters were set as follows: 100-kHz sampling rate; best-frequency resolution of 50 Hz (from 125 to 5000 Hz).

Three model parameters [AN spontaneous rates: 0.1 (low spontaneous rate, LSR), 4 (middle spontaneous rate, MSR), and 100 (high spontaneous rate, HSR) spikes/s; best modulation frequencies (BMFs): 16, 32, 64, 128, and 256 Hz; center frequencies (CFs): 0.125–1.5, 1.5–5 kHz] had been tested and model FFR of each parameter combinations. Prediction indices (PIs) of FFR_{Env} and FFR_{TFS} were calculated as Pearson correlation coefficients between real FFR waveforms and simulated FFR waveforms, respectively. The optimized parameter combinations were conducted into the ideal FFR model.

Statistical analyses were performed with MATLAB (MathWorks, Natick, MA, USA). Pairwise t-tests were conducted and the null-hypothesis rejection level was set at 0.05.

3 Results

Based on our previous study [25], an effective IC FFR model should be able to separate FFR_{Env} and FFR_{TFS}. In the current model, spike trains output within all CF channels (from 125 to 5000 Hz) from CN-IC BP model showed relative long periodicity (Figure 2(a)) while those from CN-IC BR showed relative short periodicity (Figure 3(a)). In that case, the simulated FFR_{Env} and FFR_{TFS} (Figures 2(b) and 3(b)) differed in their spectra (Figures 2(c) and 3(c)): the spectra of simulated FFR_{Env} distributed mainly below 640 Hz (same frequency range of the acoustic envelope), while the spectra

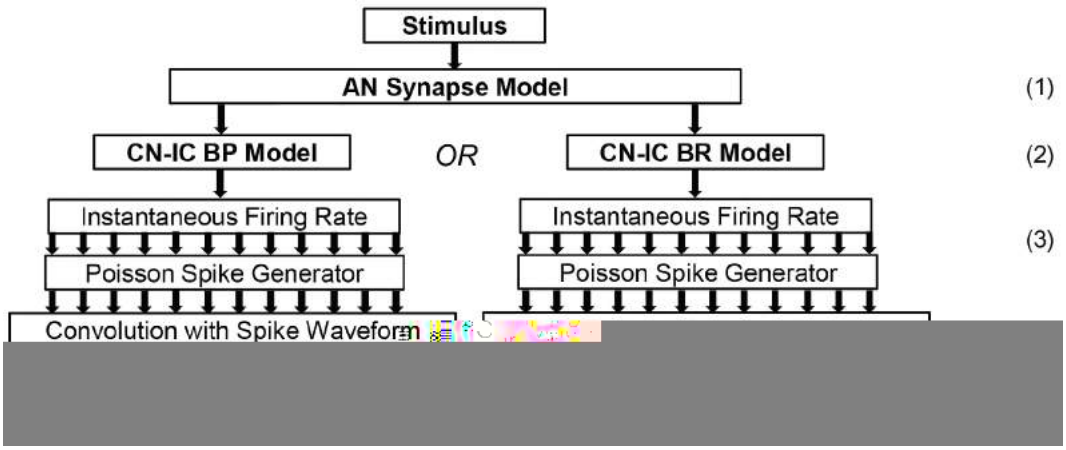

Figure 1 Schematic of the model structure of the inferior colliculus (IC) originated FFR_{Env} and FFR_{TFS}, respectively. (1) An existing auditory peripheral model (auditory nerve model [41]) was used to provide inputs to higher neural center (frequency channels centered from 125 to 5000 Hz, Δf = 50 Hz). (2) Then, at CN-IC level, band-pass (BP) and band-reject (BP) models [38] were used to separate the envelope and TFS information. (3) The instantaneous firing rate of each frequency channel was used to generate spike trains by fast-Poisson process [42]. (4) The spike trains were then convolved with a model spike waveform to get the field potentials. (5) Finally, the simulated FFRs were summed cross all the potential in frequency channels, with 100 independent repetitions. IC, inferior colliculus; IHC, inner hair cell; AN, auditory nerve; CN, cochlear neulus; BP, band-pass; BR, band-rejected.

Figure 2 The raw FFR_{Env} model outputs under different best modulation frequency (BMF) conditions (high spontaneous rates of modeled AN fbers). (a) Spike trains in all frequency channels (from 125 to 5000 Hz); (b) waveforms of model FFR_{Env}; (c) spectra of model FFR_{Env}. AN, auditory nerve.

Figure 3 The raw FFR_{TFS} model outputs under different best modulation frequency (BMF) conditions (high spontaneous rates of modeled AN fbers). (a) Spike trains in all frequency channels (from 125 to 5000 Hz); (b) waveforms of model FFR_{TFS}; (c) spectra of model FFR_{TFS}. AN, auditory nerve.

simulated FFR_{TFS} distributed around 2000 Hz (same frequency range of the acoustic TFS).

As shown in Figures 2 and 3, the simulated FFRs of different BMFs differed both in their waveforms and spectra. In order to estimate the model predictive validity, PIs of FFR_{Env} and FFR_{TFS} were calculated as Pearson correlation coeffcients between real FFR waveforms and simulated FFR waveforms, respectively. Figure 4(A) presents how well the simulated FFR_{Env} and FFR_{TFS} could effectively imitate the real FFR_{Env} and FFR_{TFS} along different BMFs. Ideally, the PIs of FFR_{TFS} of model TFS should be larger than those of model envelope, while the PIs of FFR_{Env} of model envelope should be larger than those of model TFS. In the other word, in Figure 4(A), the PIs of FFR_{TFS} (circles in Figure 4(A)) should be distributed below the diagonal and the PIs of FFR_{TFS} should be distributed above the diagonal (crosses in

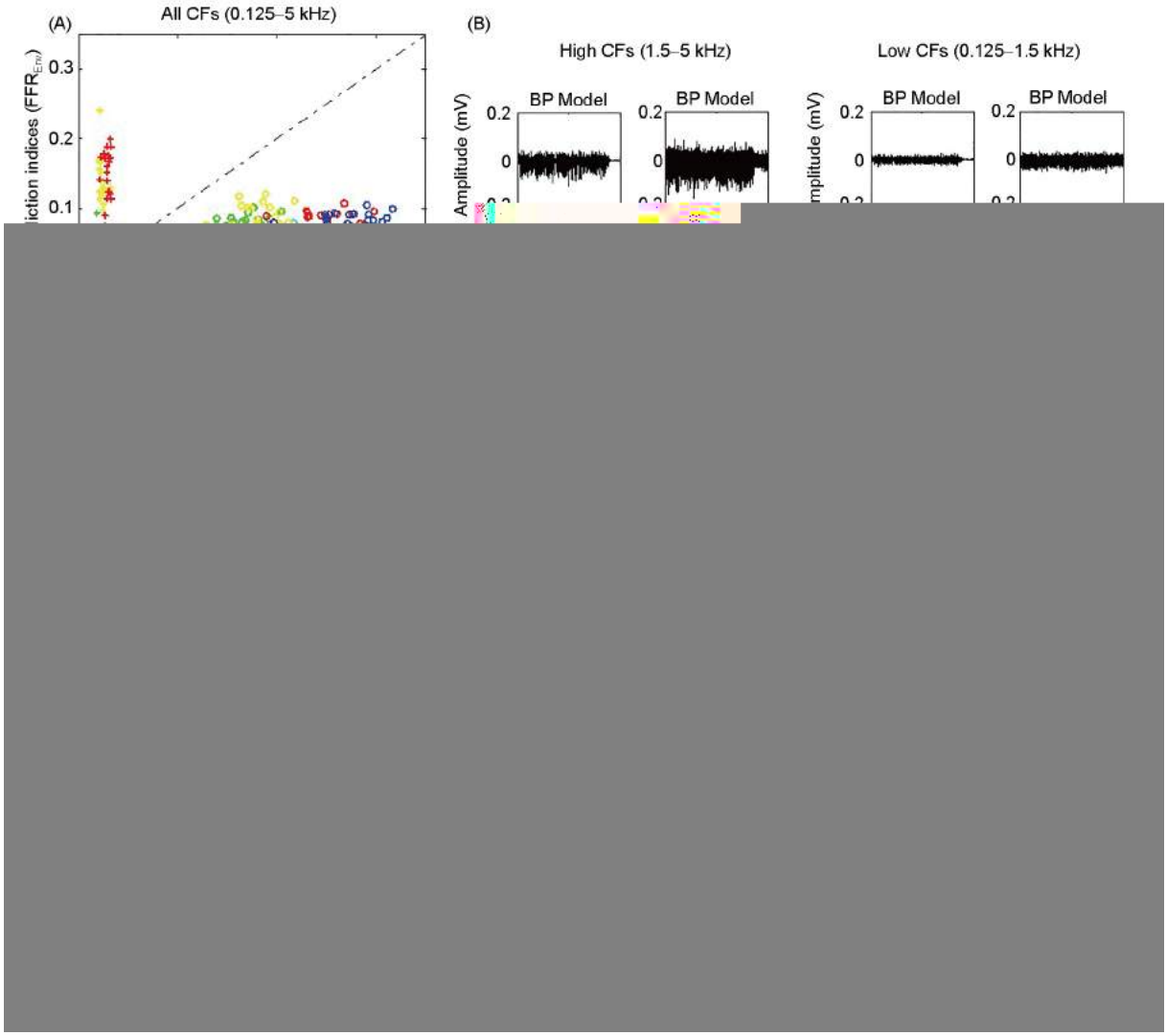

Figure 4 Illustrations of the model FFR_{Env} and FFR_{TFS} generated by low (0.125–1.5 kHz) and high (1.5–5 kHz) frequency channels only. (A) Comparison of prediction indices (PIs) of FFR_{Env} or FFR_{TFS}. For each dot, the distance from the diagonal represented the discrimination degree between FFR_{Env} or FFR_{TFS}. (B) Examples of model FFR_{Env} or FFR_{TFS} generated by low and high CFs respectively. The model FFR generated by low CFs gave quite low signal-to-noise ratio within FFR spectrum. (C) Comparisons of model predictions to experimental FFR_{Env} and FFR_{TFS} with different model parameters. The low CFs generated model FFRs gave a weak contributions to the experimental data. BMF, best modulation frequency; CFs, frequency channels; M, model.

Figure 4(A)). Furthermore, the distance from the diagonal represents the discrimination degree between FFR_{Env} and FFR_{TFS}. The top panel of Figure 4(A) shows that the current FFR model can effective simulate both FFR_{Env} and FFR_{TFS} and effectively separated the two components.

In order to choose the optimized parameters, two parameters of the current model (AN spontaneous rate: LSR, MSR, and HSR; BMF: 16, 32, 64, 128, 256 Hz) were modulated. As the previous studies [34] have suggested that high-frequency channels (from 1.5 to 10 kHz) contribute more to FFR, two different CF channels (low CFs: 0.125–1.5 kHz; high CFs: 1.5–5 kHz) were also modulated to for the comparison. The PIs of FFR_{Env} and FFR_{TFS} under each parameter combination were calculated for further analyses. As shown in Figure 4(A), PIs of model FFR_{Env} and FFR_{TFS} obtained with high frequency channels were similar to those obtained with all CF channels (0.125 5 kHz), which signi f cantly contribute to experimentally obtained FFR_{Env} and FFR_{TFS}. However, PIs of model FFR_{Env} and FFR_{TFS} obtained with low frequency channels were poor (bottom panel of Figure 4(A)). An example of simulated FFR_{Env} and FFR_{TFS} (HSR, BMF = 128 Hz) was that either FFR_{Env} or FFR_{TFS} obtained by low frequency channels were lower in the absolute amplitude of signal-to-noise ratio in spectra (Figure 4(B)). These results demonstrate that both low-frequency envelope and high-frequency TFS arise from the f ne phase-locking mechanisms in the high-frequency channels.

According to the PIs values of FFR_{Env} and FFR_{TFS}, we developed the monaural ideal FFR_{Env} and FFR_{TFS} model by averaging the outputs selections of optimized parameter

combinations. As shown in Figure 4(C), the optimized selections include two for FFR_{TFS} (HSR, BMF = 128 and 256 Hz) and four for FFR_{Env} (HSR and MSR × BMF = 64 and 128 Hz), only obtained with high CFs. Compared to PIs of raw model, PIs of ideal simulated FFR_{TFS} and FFR_{Env} were significantly higher under both ipsilaterally and contralaterally stimulated conditions (Figure 5) (paired *t*-tests, all $p < 0.05$). On the other hand, PIs of ideal simulated FFR_{TFS} and FFR_{Env} were significantly higher than PIs of raw model under both ipsilaterally and contralaterally stimulated conditions (Figure 5) (paired *t*-tests, all $p < 0.05$).

To be noted, all the experimental data used was from the central nucleus of IC in 21 out of the 24 recording sites, according to the histological examination (Figure 6).

4 Discussion

The present study investigates the roles of both auditory periphery processing (parameters: spontaneous rates and CFs) and auditory brainstem processing (parameters: BMF) for the formation of FFR_{Env} and FFR_{TFS}, respectively. According to our previous intracranial FFR recording studies in the rat IC

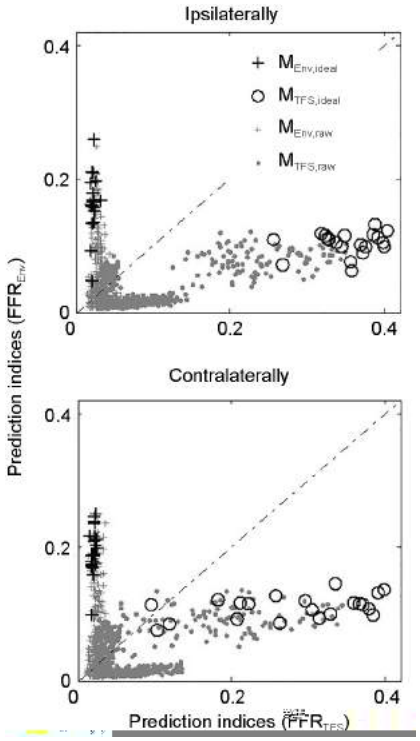

Figure 5 Outputs of the monaural ideal FFR_{Env} and FFR_{TFS} model. Four optimized parameter combination (HSR, MSR × BMF = 64, 128 Hz) were chosen for the ideal FFR_{Env} model while two (HSR, BMF = 128, 256 Hz) were chosen for the ideal FFR_{TFS} model. For each data, the distance from the diagonal represented the discrimination degree between FFR_{Env} and FFR_{TFS}. Compared to the raw model data, the ideal FFR model predictions to ipsilateral FFR_{TFS} and contralateral FFR_{Env} was significantly improved.

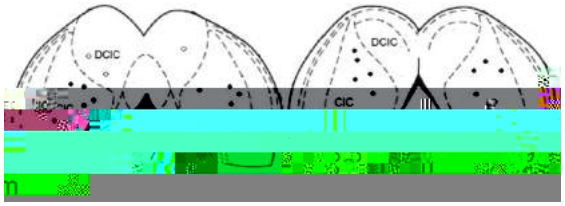

Figure 6 Histological results of recording electrodes in 12 rats. Electrodes were precisely located within the central nucleus of the inferior colliculus (IC) in 21 of the 24 penetrations (filled circles and the star). Note that two electrodes were inserted per animal, one on each side of the IC.

[25],

from his previous study [44] in order to predict the scalped recorded FFRs. While in the current study, the unitary response function is calculated as a model spike waveform k, which is approximated with a Gabor function [36,45] in order to predict the intracranial recorded FFRs. Comparing with Kuokkanen's FFR model [36], the advantages of the new developed model is the ability to separate neural TFS and envelope components by a phenomenological modeling approach. Furthermore, because the Kuokkanen's FFR model [36] is established for birds' MSO, the new developed model which is established for rats' IC might be more suitable to interpret the response patterns of FFRs in mammals. The gap between prediction of scalp FFRs and intracranial FFRs should be fxed in the future investigations.

In conclusion, an effective FFR model which explains the formation of $\mathrm{FFR_{Env}}$ and $\mathrm{FFR_{TFS}}$ is developed. This model can be further applied to different forms of hearing disorder to understand what stages the impairments of FFR generation happen.

We thank Laurel Carney for discussion and for critical reading of an earlier version of this paper. This work was supported by the National Natural Science Foundation of China (Grant No. 31470987), the National Basic Research Development Program of China (Grant No. 2015CB351800), "985" grants from Peking University for Physiological Psychology and China Postdoctoral Science Foundation (Grant No. 2016M601066).

1 Moore B C J. The role of temporal fne structure processing in pitch perception, masking, and speech perception for normal-hearing and hearing-impaired people. J Assoc Res Oto, 2008, 9: 399–406
2 Rosen S. Temporal information in speech: Acoustic, auditory and linguistic aspects. Philos Trans R Soc B-Biol Sci, 1992, 336: 367–373
3 Smith Z M, Delgutte B, Oxenham A J. Chimaeric sounds reveal dichotomies in auditory perception. Nature, 2002, 416: 87–90

(*Tyto alba*). J Neurophysiol, 2010, 104: 2274–2290
37 Langner G, Schreiner C E, Biebel U W. Functional implications of frequency and periodicity coding in auditory midbrain. In: Palmer A R, Rees A, Summerfeld A Q, et al., eds. Psychophysical and Physiological Advances in Hearing. London: Whurr Publ. Ltd., 1998. 277–285
38 Carney L H, Li T, McDonough J M. Speech coding in the brain: Representation of vowel formants by midbrain neurons tuned to sound fluctuations. eNeuro, 2015, 2
39 Paxinos G, Watson C, Carrive P, et al. Chemoarchitectonic Atlas of the Rat Brain. Atlanta: Elsevier, 2009
40 Longtin A, Middleton J W, Cieniak J, et al. Neural dynamics of envelope coding. Math Biosci, 2008, 214: 87–99
41 Zilany M S A, Bruce I C, Carney L H. Updated parameters and expanded simulation options for a model of the auditory periphery. J Acoust Soc Am, 2014, 135: 283–286
42 Jackson. The SGfast Mex Function. https://www.urmc.rochester.edu/MediaLibraries/ URMCMedia/labs/carney-lab/documents/articles/Jackson-SGfast-2003.pdf, 2003
43 Goldstein Jr. M H, Kiang N Y S. Synchrony of neural activity in electric responses evoked by transient acoustic stimuli. J Acoust Soc Am, 1958, 30: 107–114
44 Dau T, Wegner O, Mellert V, et al. Auditory brainstem responses with optimized chirp signals compensating basilar-membrane dispersion. J Acoustical Soc Am, 2000, 107: 1530–1540
45 Gold C, Henze D A, Koch C, et al. On the origin of the extracellular action potential waveform: a modeling study. J Neurophysiol, 2006, 95: 3113–3128